International Journal for Multidisciplinary Research (IJFMR)
E-ISSN: 2582-2160 ● Website: www.ijfmr.com ● Email: editor@ijfmr.com

Computational Insights on Electronic Structure, Spectral Characteristics of Aminonaphthoquinone Derivatives

Maneesha N Shewale

Department of Chemistry, Baburaoji Gholap College, Sangvi, Pune-411027.

Abstract:
The alkyl amino derivatives of 1,4-naphthoquinones exhibit interesting chemical and biological characteristics, including anticancer activities. Dispersion corrected M06-2X based density functional theory has been employed to characterize electronic structures and UV-visible spectra of 2-chloro-3-(n-alkylamino)- 1,4-naphthoquinone and 2-bromo-3-(n-alkylamino)- 1,4-naphthoquinones (alkyl: methyl, ethyl, propyl and butyl) to study the effect of increasing alkyl chain.
These molecules are stabilised through intramolecular hydrogen bonding which reflects in the characteristic N–H vibrational frequency appearing at ~3300 cm^{-1}. Underlying hydrogen bonding interactions are analyzed through MESP topography and non-covalent interaction (NCI) analyses. Frontier orbital analyses reveal that the HOMO is localized over the substituted amine moiety of naphthoquinones derivatives. In addition, better intermolecular interactions were observed by Hirshfeld surface analysis.

Keywords: aminonaphthoquinone, Density Functional Theory, MESP, hirshfeld analysis

1. Introduction

Traditional chemotherapy often faces limitations due to its lack of selectivity, which can cause medications to affect non-target tissues and result in adverse side effects [1]. Consequently, there is an urgent need for more potent, tissue-specific therapeutic agents. This need is further compounded by the escalating resistance of bacterial and fungal pathogens to existing antibiotics, necessitating alternative strategies to bypass traditional resistance mechanisms [2]. The National Cancer Institute (NCI) has highlighted the quinone group as an essential pharmacophore for inducing cytotoxic activity [3]. Quinones are prevalent in nature and form the core of several clinically approved drugs, including: Anthracyclines (e.g., Doxorubicin, Daunorubicin), Mitomycin and Saintopin. The cytotoxicity of quinones is primarily attributed to their interaction with DNA topoisomerase-II. They act as "topoisomerase poisons," stabilizing the covalent enzyme-DNA complex and preventing DNA religation, which results in lethal double-stranded breaks [4]. Furthermore, quinones are highly redox-active. They can undergo one-electron reductions to form semiquinones or free radicals [5]. Among the quinone family, naphthoquinone derivatives are particularly notable for their diverse pharmacological profile. Besides their cytotoxic effects, they exhibit potent antiviral, antibacterial, antifungal, anti-inflammatory, and antipyretic activities. To synthesize new drugs effectively, a deep understanding of the structural and spectral properties of these derivatives is required. The biological efficacy of 1,4-naphthoquinone derivatives is largely determined by their ability to interact with cellular targets through specific chemical substitutions. By introducing

"amino" groups, researchers can fine-tune the molecule's reactivity and binding affinity, transforming a simple quinone scaffold into a potent therapeutic agent. In case of amino-1,4-naphthoquinones, the amino group acts as a synthetic precursor and a crucial structural element in many natural products. These derivatives are known for their ability to form hydrogen bonds with biological targets, such as the active sites of enzymes [6]. The amino-1,4-naphthoquinone moiety is a structural cornerstone in both natural products and synthetic pharmacology. It serves as a key synthetic intermediate in the production of various chemicals with potential biological applications. Due to their strong antibacterial, anticancer, and antimalarial properties, the alkyl amino derivatives of 1,4-naphthoquinones are particularly important in medicinal chemistry and drug development.

Alkyl amino derivatives exhibit high potency against bacteria, cancer and malaria. Their mechanism of action involves the disruption of mitochondrial electron transport and DNA intercalation, as noted by Futuro et al. in 2018 [5].

The 2-chloro-3-(n-alkylamino)-1,4-naphthoquinone (designated as L-1 to L-4) compounds synthesized by Pawar et.al [7] represent a targeted approach to combating fungal pathogens. These derivatives have demonstrated significant antifungal and antiproliferative actions, specifically targeting three major fungal threats: Candida albicans which is the primary cause of opportunistic infections in immunocompromised patients [9]. Candida tropicalis, a highly virulent species often found in intensive care units (ICUs) [10] and Cladosporium herbarum, a widespread allergenic fungus [11].

By varying the length of the n-alkyl chain from methyl (L−1) to butyl (L−4), researchers can optimize the lipophilicity and cellular uptake of the drug, enhancing its efficacy against specific fungal strains [8]. The length of the alkyl chain plays a critical role in determining how these molecules interact with the fungal lipid bilayer. For instance, the L-1 compound, containing a methyl group ($-CH_3$), exhibits strong polar interactions and is effective against planktonic fungal cells. The L-2 compound, with an ethyl group ($-C_2H_5$), achieves a balance between lipophilicity and solubility. Increasing the chain length to a propyl group ($-C_3H_7$) in L-3 enhances membrane permeability. Among these, the L-4 compound, which has a butyl group ($-C_4H_9$), shows the strongest antiproliferative action in many assays, a result attributed to its enhanced hydrophobic binding. Thus, variations in alkyl chain length significantly influence the compounds' effectiveness by modulating their interaction with fungal membranes.

The development of homologated series 2-(n-alkylamino)-1,4-napthoquinone derivatives by Patil et. al. represents a significant intersection of medicinal chemistry and structural biology [12]. The effectiveness of these compounds is not solely dependent on their chemical formula but also on their physical dimensions and electronic behavior. The length of the alkyl chain also plays a significant role; increasing the chain length from pentyl to octyl may limit interactions with certain biomolecules, as excessive hydrophobicity can reduce solubility or cause steric hindrance [8].

The synthesis of 2-chloro-3-(n-alkylamino)-1,4-naphthoquinone derivatives highlight how subtle structural modifications—specifically the lengthening of the n-alkyl chain—drastically shift a drug's efficacy and selectivity. Methyl, ethyl, propyl, butyl derivatives L-1–L-4, then pentyl–octyl L-5–L-8 synthesized and fully characterized; prepared by direct reaction of alkylamines with 2,3-dichloro-1,4-naphthoquinone [13].

By reacting 2,3-dichloro-1,4-naphthoquinone with primary amines, a series of ligands was created that demonstrates a complex relationship between lipophilicity and biological action. The presence of the 2-chloro substituent, combined with the 3-amino group, creates a highly reactive electronic environment. These compounds function by Inducing ROS, Topoisomerase Inhibition and Ergosterol Interference. The

study confirms that these derivatives do not merely circulate in the biophase; they actively anchor to fungal structures through two key mechanisms: the intermolecular hydrogen Bonding that facilitates the initial attachment of the aminonaphthoquinone moiety to the fungal cell wall or membrane proteins. The π···π stacking interaction leads to intercalation, where the planar quinonoid rings slide between the base pairs of fungal DNA, disrupting replication [13].

While lipophilicity is essential for a drug to penetrate the lipid-rich cell membranes of fungi, the study found an inverse relationship between alkyl chain length and antifungal potency against *C. albicans*, *C. tropicalis*, and *C. herbarum*. The methyl derivative (L-1, n-methylamino) showed the highest activity. As the alkyl chain increased from methyl to butyl, the antifungal profile actually decreased. This suggests that while some lipophilicity is required for absorption, excessive chain length may cause steric hindrance or reduce the molecule's solubility in the aqueous biological environment, preventing it from reaching the target site effectively [8]. The researchers extended their investigation to human cancer cell lines, focusing on the colon, brain, and pancreas. Cancer cells originating from the colon and pancreas have shown significant sensitivity to the aminonaphthoquinone scaffold. In contrast, activity against brain (CNS) cancer cells is heavily dependent on the molecule's ability to cross the blood-brain barrier, a property influenced by the homologation of the alkyl group. The impact of homologation on the amino group is the primary driver of tissue selectivity. By adjusting the chain length, researchers can "tune" the molecule to be more or less selective for specific cancer types, potentially reducing the off-target damage to healthy tissues that plagues traditional chemotherapy [1].

The synthesis and structural diversity of 2-bromo-3-(n-alkylamino)-1,4-naphthoquinone derivatives, as revealed by X-ray crystallography, demonstrates how slight changes in the alkyl chain (homologation) drastically reorganize the molecular architecture [14]. These structural shifts directly influence how the compounds interact with biological targets and how they behave during redox processes. The organization of these molecules in a solid state provides a blueprint for their stability and reactivity. The study highlights three distinct structural motifs based on the alkyl substituent: The presence of an ethyl group facilitates N-H···O interactions that link individual molecules into a continuous, one-dimensional polymeric chain. As the chain length increases to propyl, the bonding pattern shifts. A combination of X-H···O (X=O, C) hydrogen bonding creates a "ladder" configuration, increasing the structural complexity and rigidity of the assembly.

It is noteworthy that quinonoids from adjacent chain rings interact through π–π interactions, resulting in the formation of alternating dimeric chains. This emphasizes that the interactions between the homologated series and biomolecules are strongly influenced by both non-covalent and π–π stacking interactions, which contribute to variations in their biological activity and redox behavior [14].

The aminonaphthoquinones derivatives used in studied herein are:

a)	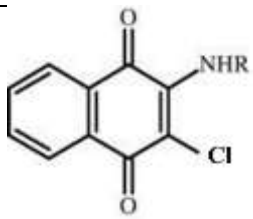	L1Br: R1 = CH_3 L2Br: R2 = C_2H_5 L3Br: R3 = C_3H_7 L4Br: R4 = C_4H_9

b)	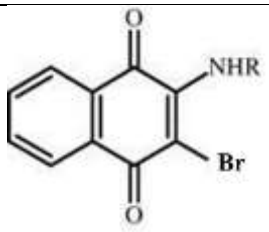	L1Cl: R1 = CH_3 L2Cl: R2 = C_2H_5 L3Cl: R3 = C_3H_7 L4Cl: R4 = C_4H_9

Figure 1. Molecular structures a) 2-(n-alkylamino)-3-chloro-naphthalene-1,4-dione and b) 2-(n-alkylamino)-3-bromo-naphthalene-1,4-dione

2. Computational Methodology

The geometry optimization of the all four 2-(n-alkylamino)-3-chloro-naphthalene-1,4-dione and 2-(n-alkylamino)-3-bromo-naphthalene-1,4-dione derivatives (4a, 4b, 4c and 4d) was carried out M06-2X hybrid meta-GGA exchange-correlation functional based DFT in conjugation with the internally stored 6-31+G(d,p) Gaussian basis set employing the Gaussian 09 suite of programs.[15] The lack of imaginary frequencies indicates that the stationary points are associated with minima on PES. The assignment of normal vibrations was accomplished by observing atomic displacements relative to their equilibrium positions through Gaussview-5 software. The reactive sites and charge distribution in the derivatives was investigated using molecular electrostatic potential (MESP) [16]. The Multiwfn [17] and the visual molecular dynamics (VMD) program package [18] were utilized to perform the NCI-RDG interpretation [19]. All the calculations were carried out for the optimized structure in the gas phase.

3. Results and discussion

3.1 Geometry Optimisation

Optimized structures of 2-chloro-3-(n-alkylamino)- 1,4-naphthoquinone and 2-bromo-3-(n-alkylamino)-1,4-naphthoquinones (alkyl: methyl, ethyl, propyl and butyl) obtained from M06-2X/6-31+G(d,p) theory are depicted in Figure 2.

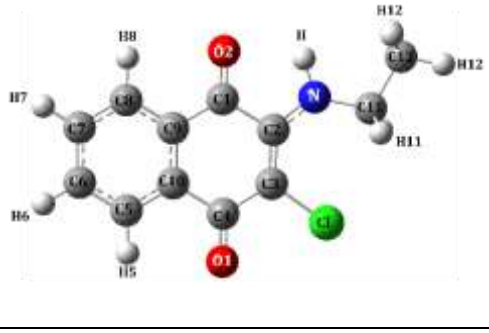	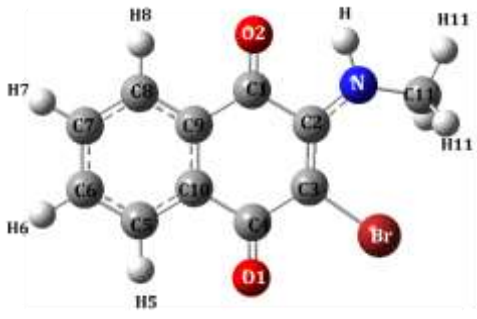
L1Cl	**L1Br**
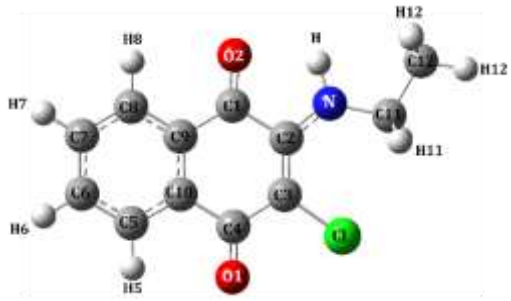	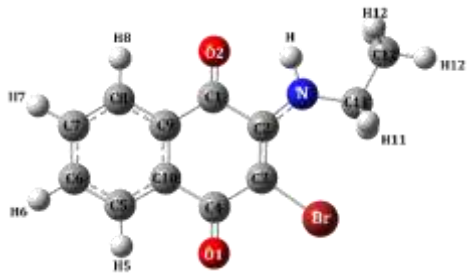
L2Cl	**L2Br**

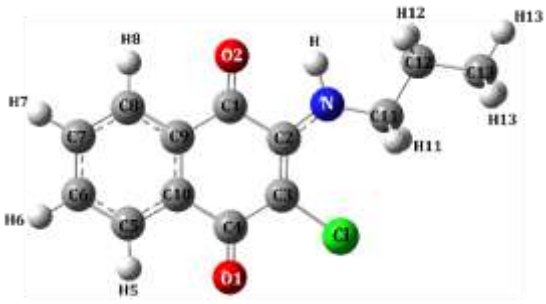

L3Cl

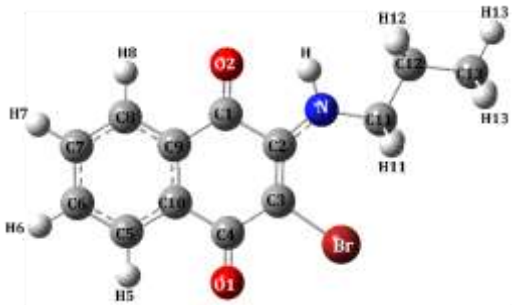

L3Br

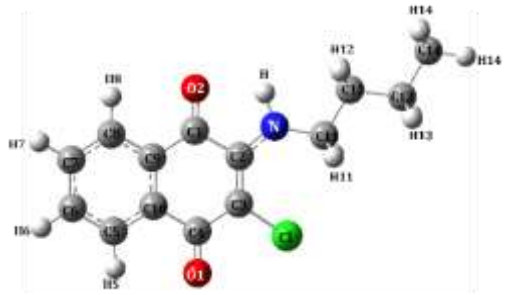

L4Cl

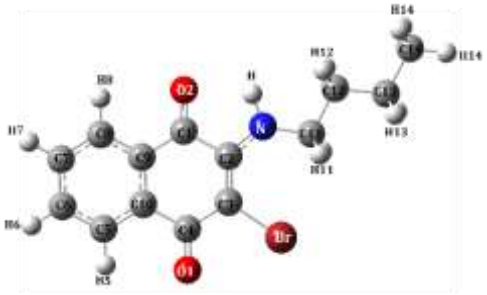

L4Br

Figure 2: Optimized geometries of L1Cl to L4Cl and L1Br to L4Br

The molecules possess C1 point group symmetry. The computed theoretical bond length (Å) along with bond angle (°) calculated M06-2X/6-31+G(d,p) theory for compounds are presented in Table 1.

Table 1. Theoretical bond length (Å) and bond angle °obtained from B3LYP method using 6-311G++ basis set

	L1Cl	L2Cl	L3Cl	L4Cl	L1Br	L2Br	L3Br	L4Br
C1-C2	1.522	1.522	1.522	1.522	1.526	1.526	1.526	1.527
C2-C3	1.369	1.369	1.369	1.369	1.368	1.369	1.369	1.369
C3-C4	1.470	1.470	1.469	1.470	1.468	1.468	1.468	1.468
C1-C9	1.479	1.479	1.479	1.479	1.477	1.478	1.478	1.478
C8-C9	1.395	1.395	1.395	1.395	1.396	1.396	1.395	1.395
C5-C6	1.393	1.393	1.393	1.393	1.393	1.393	1.393	1.393
C6-C7	1.397	1.397	1.397	1.397	1.397	1.397	1.397	1.397
C7-C8	1.391	1.391	1.391	1.391	1.391	1.391	1.391	1.391
C5-C10	1.392	1.392	1.392	1.392	1.392	1.392	1.392	1.392
C9-C10	1.397	1.397	1.397	1.397	1.396	1.396	1.396	1.396
C1-O2[a]	1.217	1.217	1.217	1.217	1.217	1.217	1.217	1.217
C4-O1	1.218	1.218	1.218	1.218	1.218	1.218	1.218	1.219
C3-Cl	1.737	1.738	1.738	1.737	---	---	---	---
C3-Br	---	---	---	---	1.884	1.885	1.886	1.885
C5-H5	1.085	1.085	1.085	1.085	1.085	1.085	1.085	1.085
C6-H6	1.085	1.085	1.086	1.086	1.085	1.086	1.086	1.086
C7-H7	1.085	1.085	1.085	1.085	1.085	1.085	1.085	1.085
C8-H8	1.085	1.085	1.085	1.085	1.085	1.085	1.085	1.085

C2-N	1.345	1.345	1.345	1.346	1.345	1.344	1.344	1.344
N-H[a]	1.013	1.015	1.015	1.015	1.013	1.015	1.015	1.015
N-C11	1.453	1.460	1.459	1.459	1.454	1.460	1.459	1.459
C11-H11	1.091	1.094	1.095	1.095	1.091	1.093	1.094	1.094
C11-C12	---	1.522	1.524	1.523	---	1.522	1.524	1.523
C12-H12	---	1.094	1.097	1.099	---	1.094	1.097	1.099
C12-C13	---	---	1.526	1.527	---	---	1.526	1.527
C13-H13	---	---	1.094	1.097	---	---	1.094	1.097
C13-C14	---	---	---	1.527	---	---	---	1.527
C14-H14	---	---	---	1.095	---	---	---	1.095
NH…O2	2.049	2.057	2.055	2.060	2.031	2.032	2.035	2.037
O2-C1-C2-N	0.2	0.8	0.5	0.8	0.8	0.0	0.8	0.0
[a] Participating in hydrogen bonding								

The C-Br bond distances fall in the range 1.885 to 1.884 Å while the C- Cl are about 1.738 Å. It was noticed that the C=N bond length is 1.345 Å. The O2-C1-C2-N dihedral angle is less than 1°.

3.2 Molecular Electrostatic Potential (MESP)

The Molecular Electrostatic Potential (MESP) topography provides insight into the charge distribution within molecules. To directly visualize electrophilic and nucleophilic regions, the MESP is mapped onto electron density isosurfaces at 0.001 atomic units (au), as shown in Figure 3. The color scheme of the MESP isosurfaces reflects charge variations: red indicates electron-rich (partially negative) areas, blue highlights electron-deficient (positively charged) regions, yellow represents slightly electron-rich zones, and light blue marks fairly electron-deficient areas. The presence of green color in the MESP isosurfaces indicates a potential value intermediate between the electron-rich red regions and the electron-deficient blue regions. The images show bright red areas around one carbonyl oxygen, signifying electron-rich regions attributed to its lone pairs, acting as electron donors. In contrast, the other carbonyl oxygen displays a yellow-red hue, indicating reduced electron density, which supports the formation of intramolecular hydrogen bonding with an N-H hydrogen. The hydrogens attached to C-H groups exhibit a light blue color, while the N-H hydrogens appear dark blue, reflecting the influence of the electronegative nitrogen atom to which they are bonded.

Further quantitative assessment of the positive and negative electrostatic potentials on the surfaces can be executed from the V_{max} and V_{min} parameters. The values are displayed in Table 2

Table 2. V_{min} and V_{max} parameters in kJmol^{-1}.

	Vmin	Vmax
L1Cl	-175.2	164.1
L2Cl	-176.3	134.6
L3Cl	-177.5	131.6
L4Cl	-177.1	130.0
L1Br	-172.9	163.4
L2Br	-174.6	132.1

L3Br	-175.7	129.7
L4Br	-175.8	129.1

V_{min} values at the carbonyl oxygen O1 in L1Cl to L4Cl are observed to be around -175 $kJmol^{-1}$ and ~ -177 $kJmol^{-1}$ for the bromo series. High values V_{max} values 164.1 $kJmol^{-1}$ and 163.4 $kJmol^{-1}$ are noticed in the L1Cl and L1Br molecules with methyl substituent. The value goes on decreasing with increasing alkyl chain length.

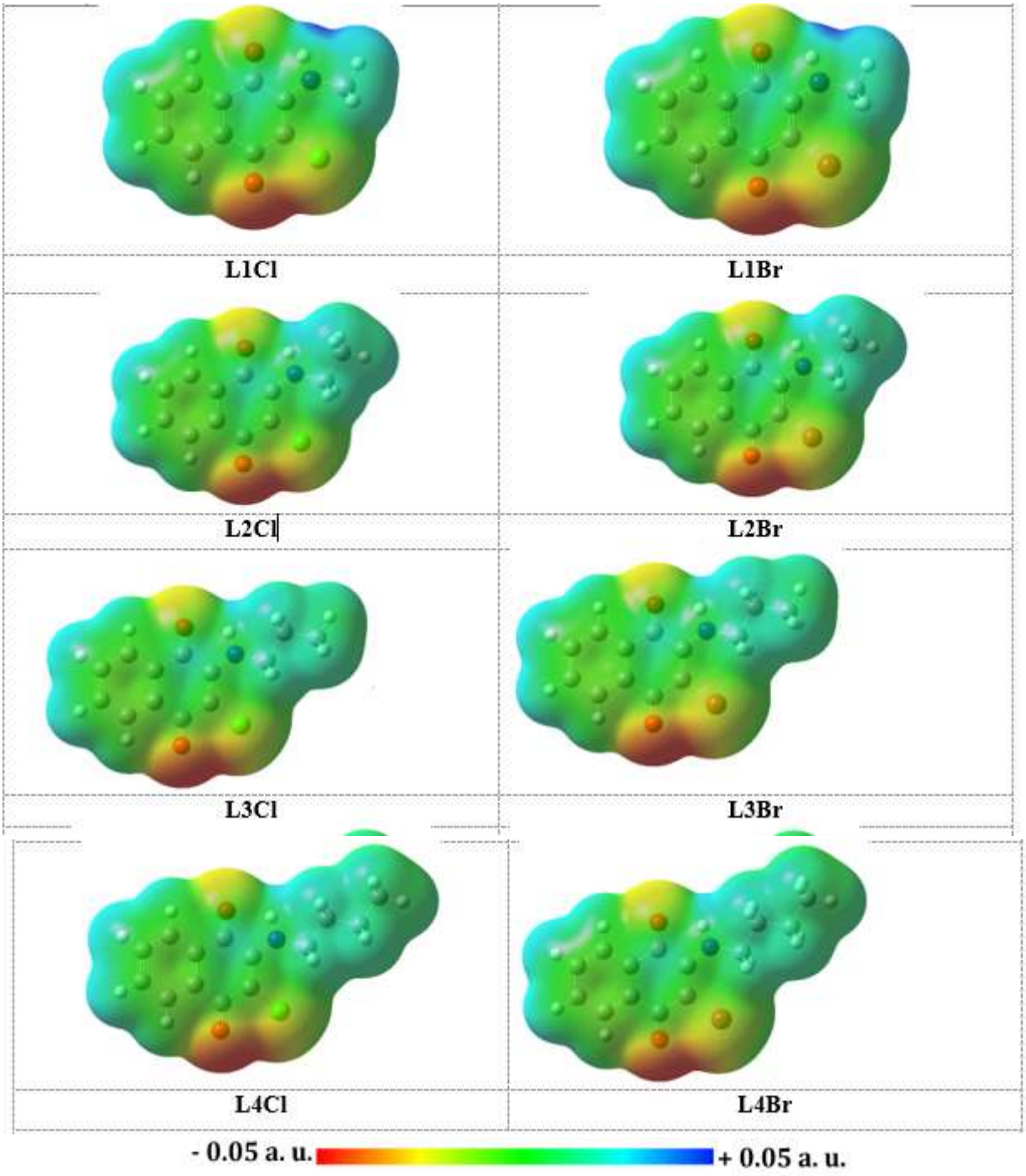

Figure 3. Electron Density isosurfaces(0.001 a.u.) overlaid with the MESP (-0.05 to +0.05 a.u.)

3.3 Frontier Orbitals

The frontier molecular orbitals, namely the Highest Occupied Molecular Orbital (HOMO) and the Lowest Unoccupied Molecular Orbital (LUMO), for the chloro and bromo compounds are illustrated in Figures 4 and 5. In the chloro derivatives, the HOMOs are predominantly localized around the chlorine atom and the aminoalkyl group, while the LUMOs are mainly distributed over the naphthalene moiety. Similar patterns are observed for the bromo derivatives. The HOMO–LUMO energy values, along with global reactivity indices such as chemical potential (μ), hardness (η), and electrophilicity index (ω), as well as thermodynamic parameters, are summarized in Table 3. A large HOMO–LUMO energy gap (ΔEg) indicates a system's resistance to electron acceptance at the LUMO and electron removal from the HOMO, thereby conferring electronic stability to the molecular system.

Table 3. HOMO, LUMO gap (in eV) and global indices in the amino naphthoquinone derivatives

Molecular properties	L1Cl	L2 Cl	L3 Cl	L4 Cl	L1Br	L2Br	L3Br	L4Br
E_{HOMO}	-7.48	-7.45	-7.53	-7.52	-7.42	-7.37	-7.36	-7.35
E_{LUMO}	-2.28	-2.26	-2.29	-2.29	-2.29	-2.27	-2.25	-2.25
$\Delta E_{HOMO-LUMO}$	-5.20	-5.19	-5.19	-5.19	-5.12	-5.11	-5.11	-5.10
Global Hardness(ŋ)	2.60	2.60	2.59	2.60	2.56	2.55	2.55	2.55
Softness (S)	0.19	0.19	0.19	0.19	0.20	0.20	0.20	0.20
Electronic chemical potential (μ)	-4.88	-4.86	-4.84	-4.84	-4.85	-4.82	-4.81	-4.80
Electronegativity (χ)	4.88	4.86	4.84	4.84	4.85	4.82	4.81	4.80
Global electrophilicity index (ω)	4.58	4.54	4.52	4.51	4.60	4.55	4.53	4.51

Frontier orbitals HOMO (Highest occupied molecular orbital) and LUMO (Lowest unoccupied molecular orbital) portrayed in Figure. 4 for the chloro derivatives revealed HOMOs are largely localized around the cholrine atom and aminoalkyl group. Moreover, the LUMO distributes over the naphthalene moiety. Similar observations are noticed for bromo derivatives.

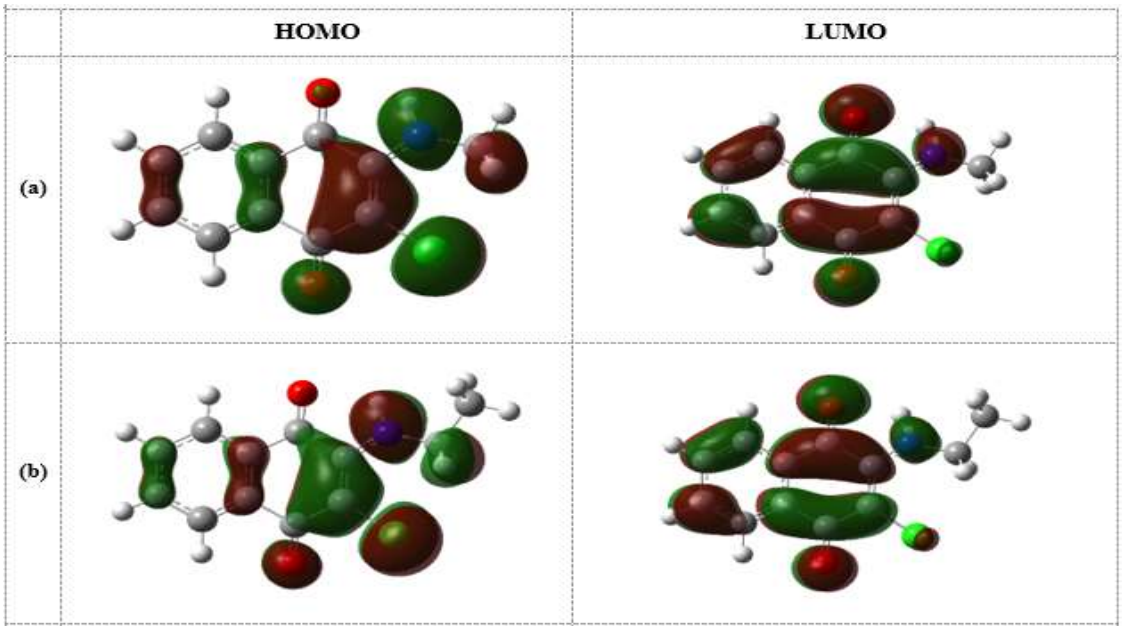

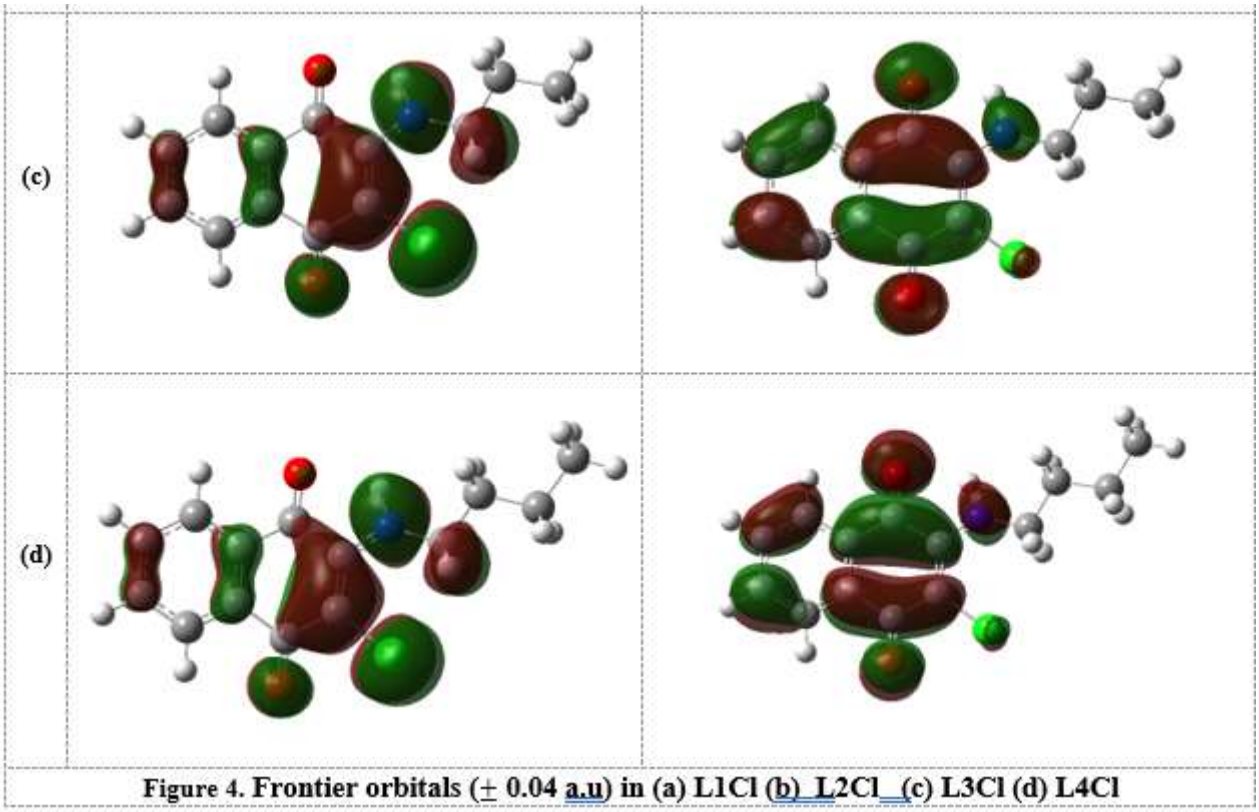

Figure 4. Frontier orbitals (± 0.04 a.u) in (a) L1Cl (b) L2Cl (c) L3Cl (d) L4Cl

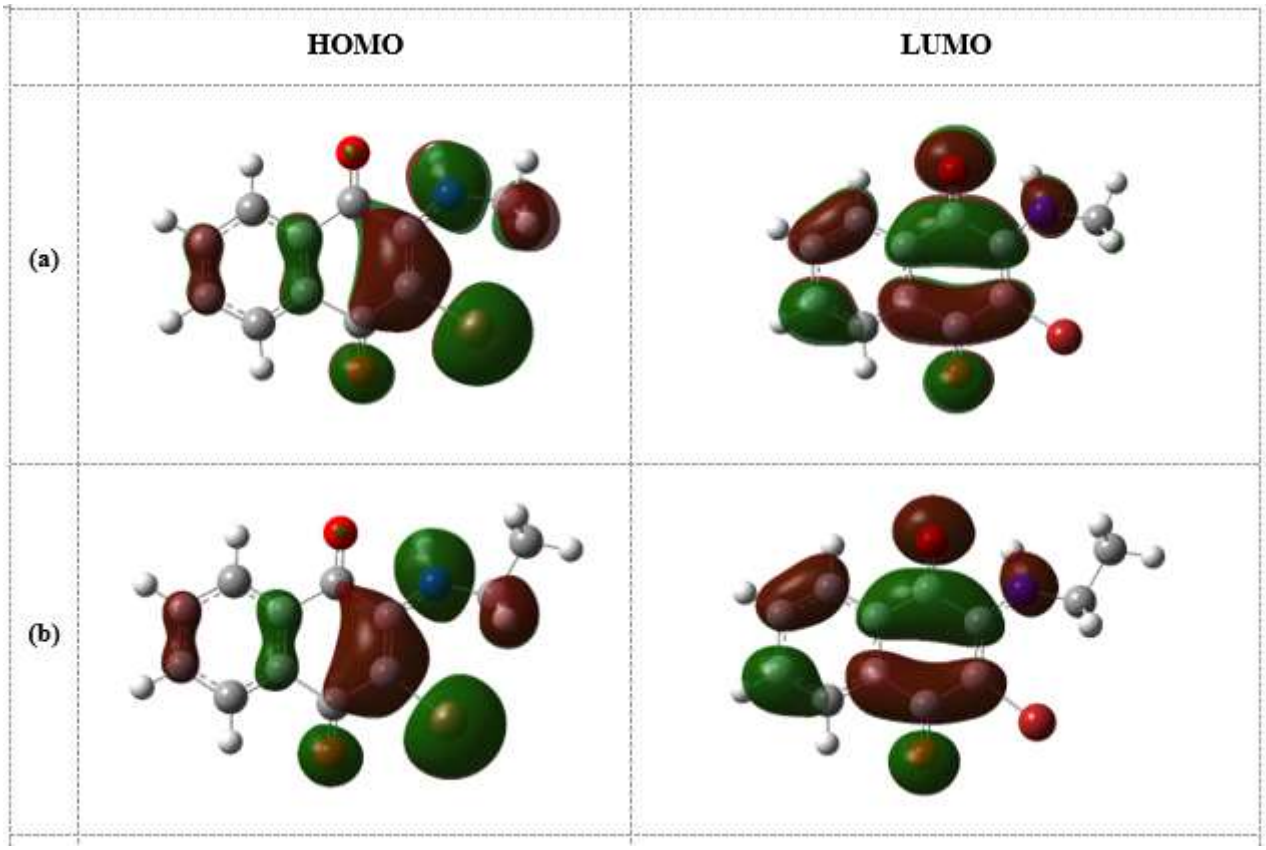

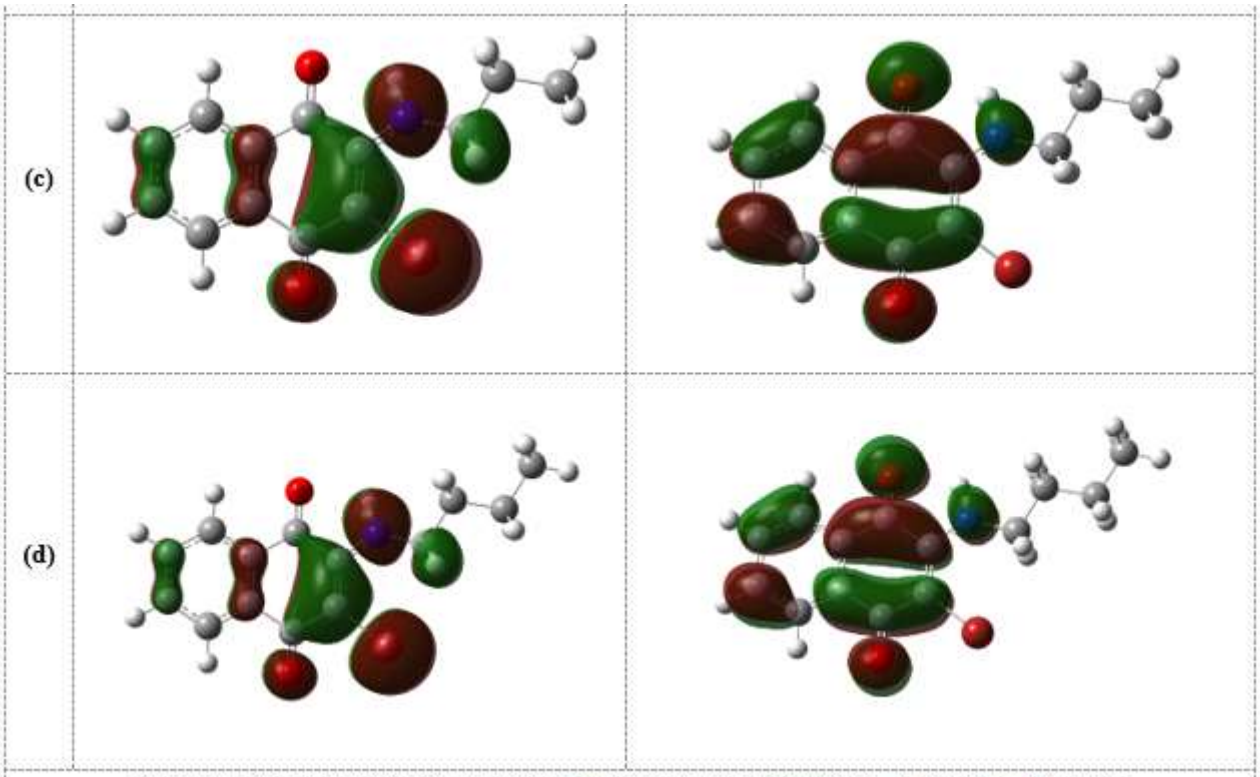

Figure 5. Frontier orbitals (± 0.04 a.u) in (a) L1Br (b) L2Br (c) L3Br (d) L4Br

3.4 Noncovalent Interaction Reduced Density Gradients (NCI-RDG)

For further ramifications of intramolecular noncovalent interactions underlying the derivatives the NCI-RDG method based on bonding topology is described. The NCI method explicates not only the attractive weak dispersive interactions but also the repulsive steric interactions in real-space via graphical representation. For 3D visualization, a pictorial representation of NCI isosurfaces for the derivatives is revealed in Figure 6. The color coding scheme followed is: strong repulsive non-bonded overlap depicted in red, green regions indicate electrostatic interactions whilst attractive interactions are seen in blue. The red elongated-shaped surfaces are noticed along the directions of decreasing density (*cf.* the central region aromatic rings in Figure 6) represent strong destabilizing steric interactions for $\rho > 0.01$ a.u. and $\lambda_2 > 0$, consequential to the strain from the ring structure where ring cohesion results from the covalent bonds. Stronger destabilized (steric crowding) interactions are confirmed from a high ρ critical value ($\rho = 0.023$ au) which show up in the aromatic rings, signified by bright red cigar-shaped surfaces. The intense peak appearing on the negative side at the sign (λ) $\rho = -0.25$ corresponds to the hydrogen bonds.

L1Cl

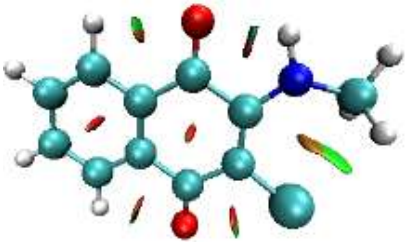

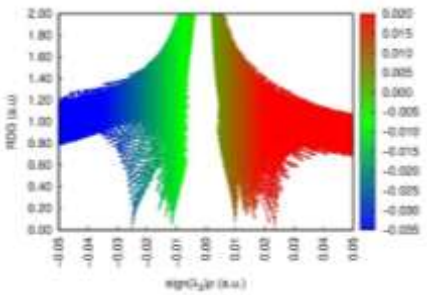

L2Cl

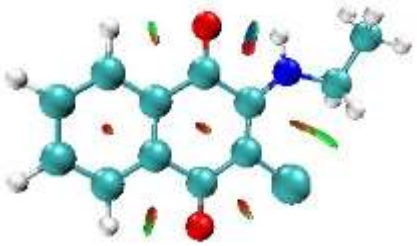

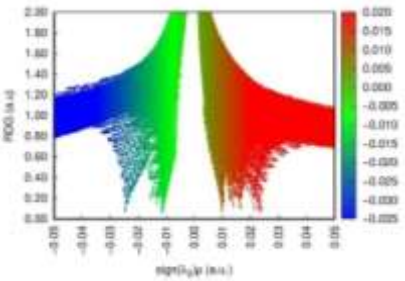

L3Cl

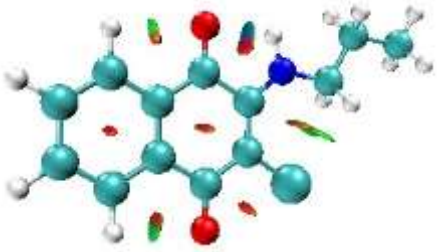

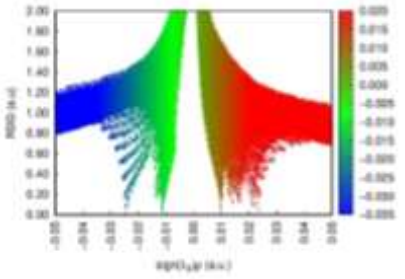

L4Cl

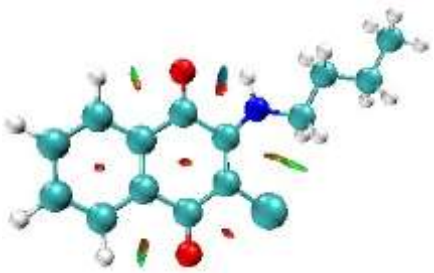

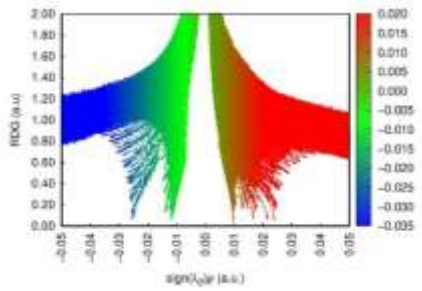

L1Br

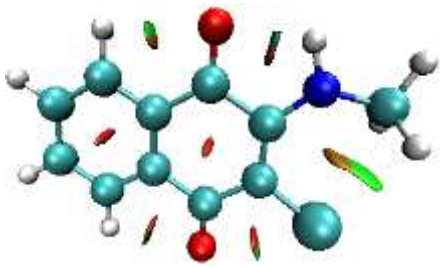

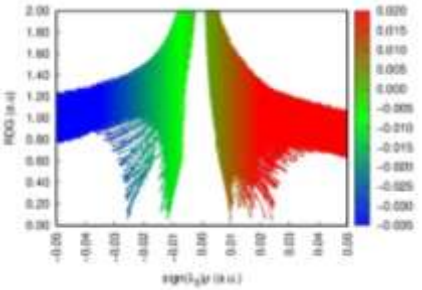

L2 Br

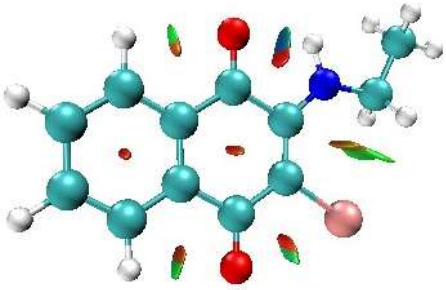

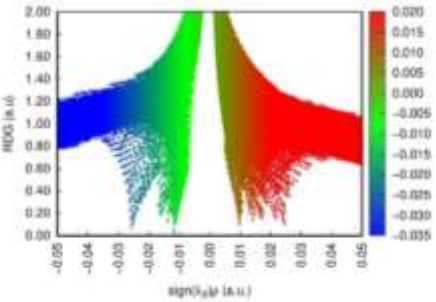

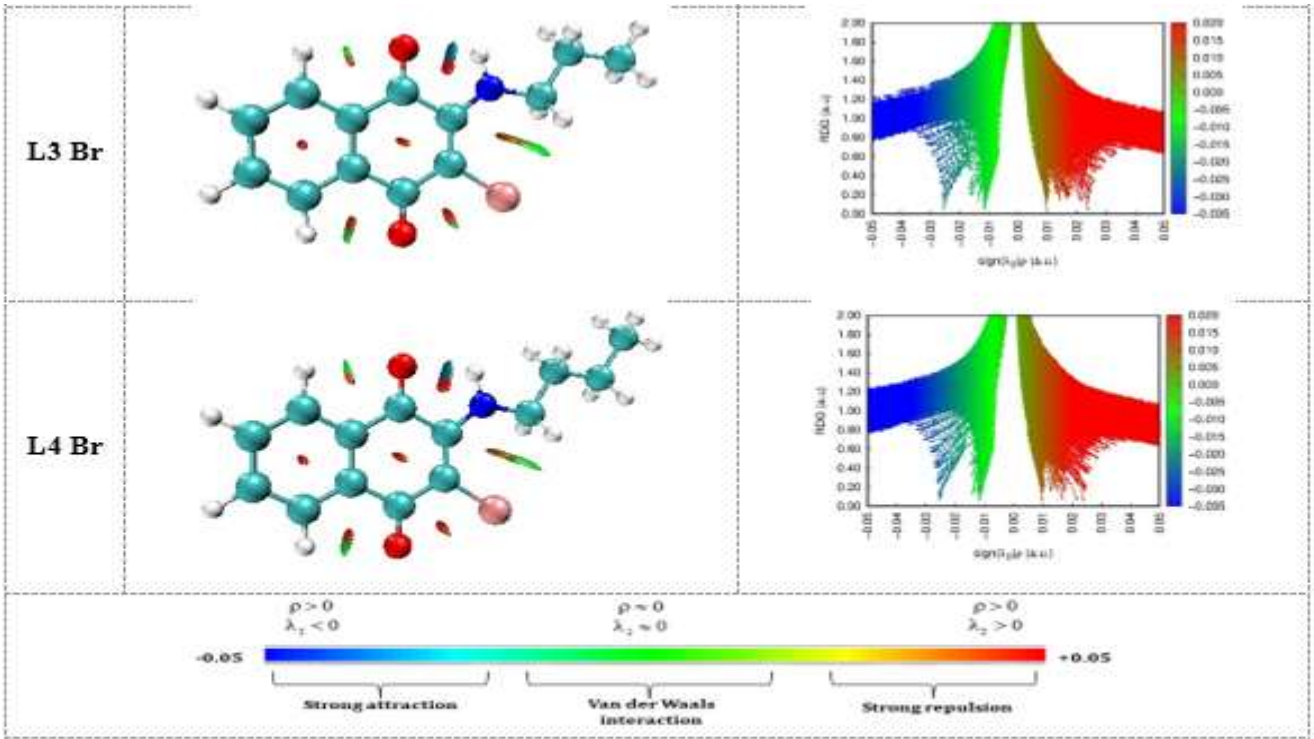

Figure 6. Color-filled RDG isosurfaces depicting noncovalent interaction (NCI) regions. Green regions refer to van der Waals interactions. The steric interactions seen in red.

3.5 Vibrational Frequencies and Natural Bond Orbital Analysis

The NBO analysis has been carried out to understand the intramolecular interactions. The redistribution of electron densities in the vicinity of inter-ionic bonds along with subsequent bond weakening and/or strengthening is apparent from the population of the corresponding localized antibonding natural orbital. The antibonding natural orbital populations (σ*) for different bonds for bromo series are displayed in Table 5 and 6. The >C=O group participating in hydrogen bonding reveal lowering in frequency with increased electron density in antibonding natural orbital (σ*). The N-H vibrations are observed at ~3400 cm^{-1} for 2-bromo-3-(n-alkylamino)-1,4-naphthoquinone derivatives. Except for L2Br, the frequency is shifted to higher wave numbers.

Table 5. Population in σ* Natural Orbitals and the corresponding bond distances in chloro series

	L1Cl			L2 Cl			L3 Cl			L4 Cl		
	σ*	r	ν	σ*	r	ν	σ*	r	ν	σ*	r	ν
N-H	0.027	1.013	3431	0.028	1.013	3402	0.029	1.015	3397	0.028	1.015	3403
C=O	0.152	1.218	1716	0.202	1.218	1706	0.203	1.218	1705	0.202	1.218	1706
C=O[a]	0.199	1.217	1732	0.153	1.217	1722	0.153	1.217	1722	0.153	1.217	1724
C-Cl	0.031	1.737	810	0.027	1.738	807	0.027	1.738	807	0.027	1.737	812

[a] Participating in hydrogen bonding

Table 6. Population in σ* Natural Orbitals and the corresponding bond distances in bromo series

	L1Br			L2Br			L3Br			L4Br		
	σ*	r	ν	σ*	r	ν	σ*	r	ν	σ*	r	ν
N-H	0.027	1.013	3408	0.029	1.015	3409	0.029	1.015	3390	0.029	1.015	3385
C=O	0.152	1.218	1716	0.204	1.218	1701	0.204	1.218	1703	0.205	1.218	1701
C=O [a]	0.199	1.217	1736	0.154	1.217	1724	0.152	1.217	1723	0.152	1.217	1723
C-Br	0.031	1.884	769	0.032	1.885	773	0.032	1.886	769	0.032	1.885	776

[a] Participating in hydrogen bonding

3.6 Hirshfeld surfaces

To investigate various molecular interactions, Hirshfeld surfaces and their associated 2D finger print plots for 2-chloro-3-(n-ethylamino)- 1,4-naphthoquinone were derived with the use of Crystal Explorer 3.1[20] employing the single crystal X-ray data. For analysis, cif∗ (Crystallographic Information File) of the compounds are used. [7,14]. The function d norm is a ratio encompassing the distances of any surface point to the nearest interior (di) and exterior (de) atom to the van der Waals radii of the atoms [21-23]. Figure 7a through 7e display surfaces those have been mapped with the dnorm, di and de visualization, shape index, curvedness and 2D finger print plots. The graphical 2D-fingerprint plots were constructed by plotting the distance external to the Hirshfeld surface (de) against the distance internal to the surface (di). A direct visual comparison imparts intense red color around the N-H substituent of the ligands which contribute largely toward N-H---O interactions (*cf.* Figure 7a). The characteristic packing modes and the ways in which the nearby molecules contact one another further gauged through shape index and curvedness parameters.

The presence of C-H···π and π-π stacking interactions in aminonaphthoquinone derivatives further are evident from the pattern of adjacent red and blue triangles those appear on the shape index surfaces and relatively large and flat green region on the same side of the molecule on the corresponding curvedness surfaces (cf. Figure 7d and 7e).

The breakdowns of finger-print plots for all such structures are illustrated in Figure 7f. From the finger-print plots, contributions from the N-H···O, C-H···O, C-H···π, CH ···N and π- π stacking interactions can be segregated. Thus, the volume (VH), area (SH), globularity (G) and asphericity ([) parameters based on hirshfield surfaces have been calculated and found to be 270.88, 254.87, 0.794 and 0.193. The term, **globularity[24]** 0.764 for the aminonaphthoquinone derivatives suggests that the molecular surface is more structured, and not a sphere. The **asphericity** [25,26] that provides measure of anisotropy. Different colors of fragment patches represent molecular interactions across the molecular region.

As seen from the Fig. 8, the most important interactions were determined with H H (35.9%), C H/H C (30.3%), N H/H N (19.8%) and O H/H O (9%) contributions.

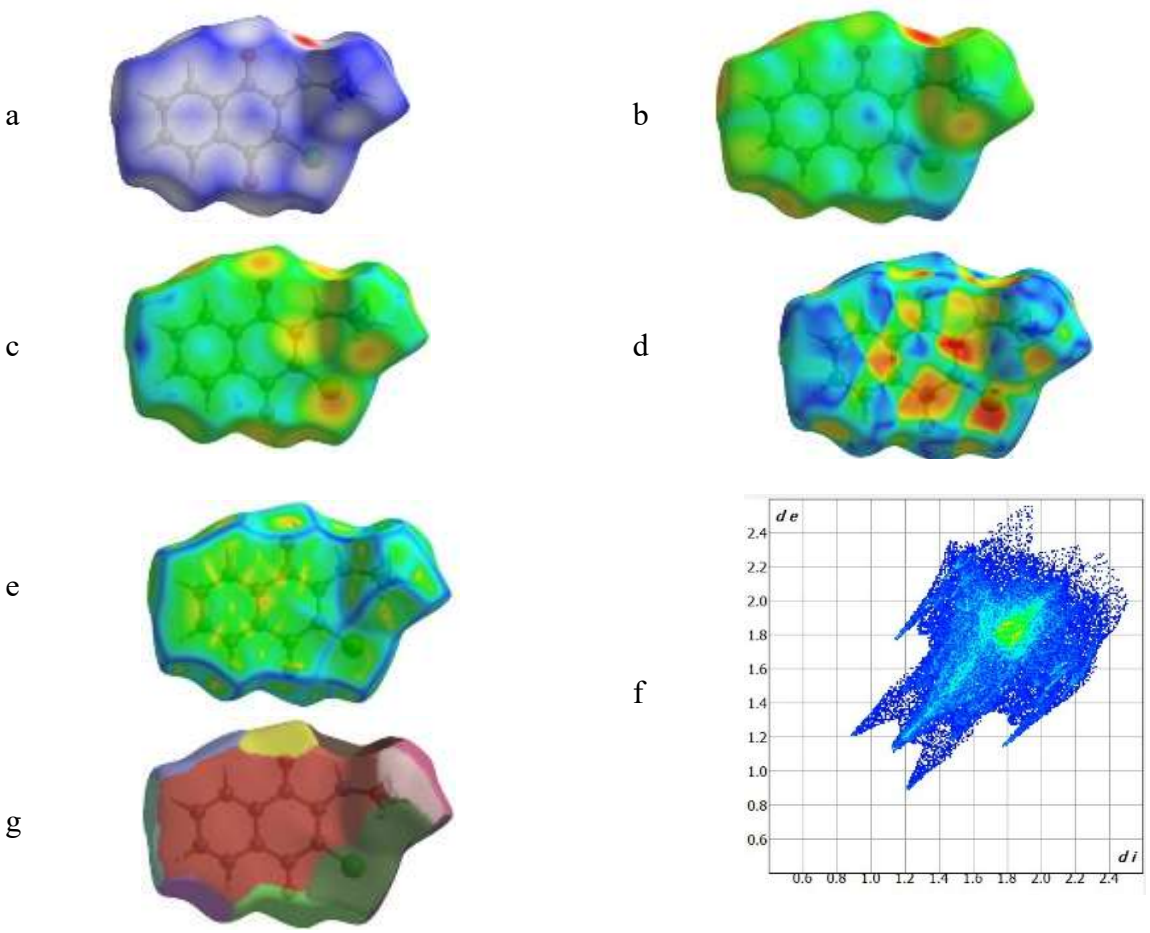

Fig. 7. Hirshfeld surface analysis: (a) dnorm visualization with red, white, and blue signify negative, zero, and positive values, (b) di visualization, (c) de visualization, (d) shape index, (e) curvedness depicting packing of molecule, (f) 2D finger print plots with di and dc ranging from 0.6 to 2.4 Å and (g) fragment patch

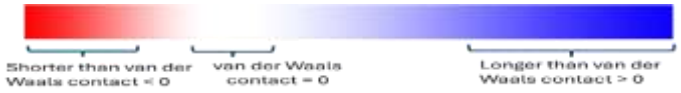

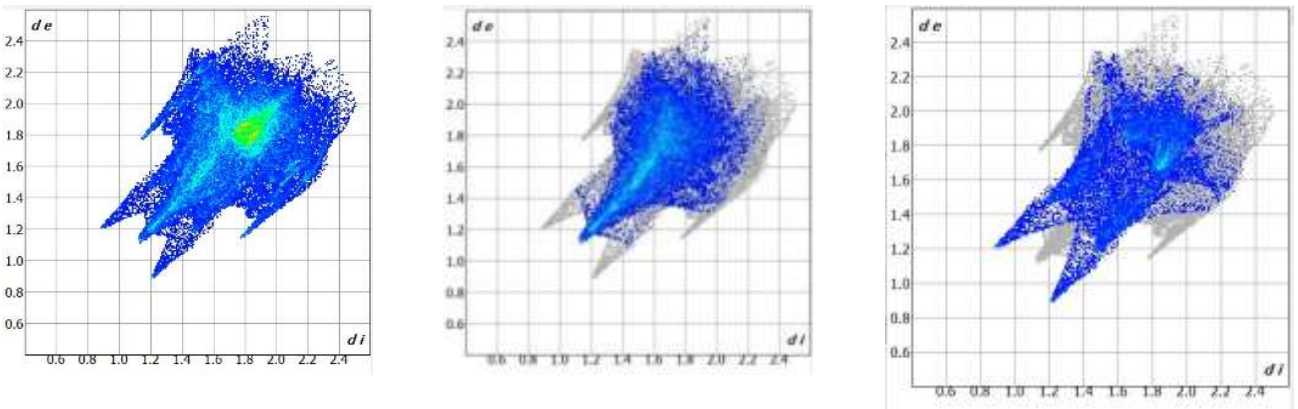

All (100%) H···H (38.1%) O–H/H···O (23.5%)

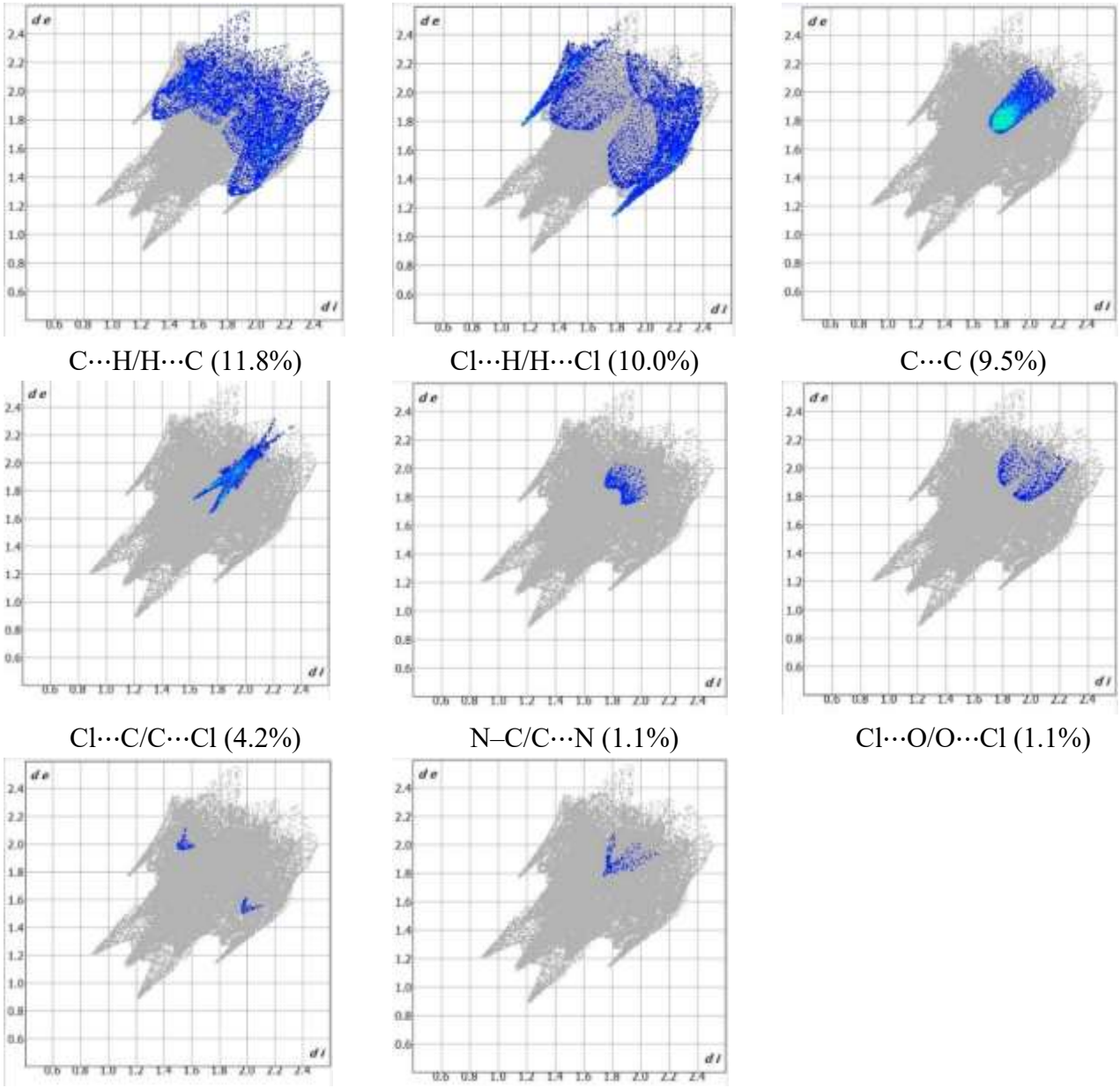

Figure 8. Two-dimensional fingerprint plots order with a dnorm view of the contacts in L2Cl. Here, di and de represent separations between the nearest atoms inside and outside to the surface, respectively

4. Conclusions:

The computational studies for the chloro and bromo compounds L-1 to L-4 indicated that an increase in the alkyl chain leads to increase in nonpolar characteristics of molecules suggesting a decrease in the antifungal activity. The increasing chain length can also hinders the interactions with biomolecules. The characteristic N–H vibrational frequency is observed at ~3300 cm^{-1}. The NBO analysis shows an increase in antibonding character for these bonds also resulting in elongation of the concerned bonds. The MESP topography puts points out to the electrophilic and nucleophilic regions which facilitates in understanding the reactive sites in the molecules. Frontier orbital analyses reveal that the HOMOs are largely localized around the cholrine atom and aminoalkyl group in the bromo derivatives. Moreover, the LUMO distributes

over the naphthalene moiety. Similar observations are noticed for bromo derivatives. Nearly 85% of the total Hirshfeld surface area in L2Cl is occupied by H···H/C/N/O/F and C···N/O contacts.

5. Acknowledgement:

The study was financially supported by the Board of College and University Development, Savitribai Phule Pune University, Pune–411007, through minor research project OSD/BCUD/83 dated 23/03/2015. The authors gratefully acknowledge the Research Centre, Baburaoji Gholap College Sangvi, Pune and S. P. Pune University, Pune for providing lab facilities and technical support.

6. References:

1. Bolton, J. L., & Dunlap T., Formation and Biological Targets of Quinones: Cytotoxic versus Cytoprotective Effects. Chemical Research in Toxicology, 2016, 30(1), 13-37.
2. de Almeida, J. D. R., et al., Antifungal potential, mechanism of action, and toxicity of 1,4-naphthoquinone derivatives. European Journal of Microbiology and Immunology, 2024,14(3), 289-295.
3. Beutler, J. A., et al., Molecular Targets Program: Heterocyclic Iminoquinones and Quinones from the National Cancer Institute. Center for Cancer Research, 2024
4. Smith E. A., et al., Etoposide Quinone Is a Covalent Poison of Human Topoisomerase IIβ. Biochemistry, 2014, 53(14), 2315-2325.
5. Futuro, D. O., et al., The Antifungal Activity of Naphthoquinones: An Integrative Review. Anais da Academia Brasileira de Ciências, 2018.
6. Rauf A., et al., Biological and pharmacological potential of anthracene-based compounds. European Journal of Medicinal Chemistry, 2015.
7. Pawar, O., Patekar, A., Khan, A., Kathawate, L., Haram, S., Markad, G., Puranik, V., & Salunke-Gawali, S., Molecular structures and biological evaluation of 2-chloro-3-(n -alkylamino)-1,4-napthoquinone derivatives as potent antifungal agents. Journal of Molecular Structure,2014, 1059, 68-74.
8. Pérez-Sacau, E., et al., Synthesis and pharmacophore modeling of naphthoquinone derivatives with cytotoxic activity in human cancer cell lines. Journal of Medicinal Chemistry, 2007, 50(4), 696-706.
9. Neto, J. B. A., et al., Antifungal activity of naphthoquinones against Candida albicans is via apoptosis. Folia Microbiologica, 2014, 59, 213–219.
10. Silva, M.C., Cardozo Bonfim Carbone, D., Diniz, P.F. et al. Modulation of ERG Genes Expression in Clinical Isolates of Candida tropicalis Susceptible and Resistant to Fluconazole and Itraconazole. Mycopathologia, 2020, 185, 675–684.
11. Tandon, V. K., et al., Synthesis and biological evaluation of novel 1,4-naphthoquinone derivatives as antiviral and antibacterial agents. European Journal of Medicinal Chemistry, 2011, 46(12)
12. Patil, R. et al. Synthesis and characterization of 2-(n-alkylamino)-1,4-napthoquinone: Molecular structures of ethyl and hexyl derivatives. Journal of Molecular Structure, 2014, 1075, 345–351.
13. Pal, S. et al. Molecular structures and antiproliferative activity of side-chain saturated and homologated analogs of 2-chloro-3-(n-alkylamino)-1,4-napthoquinone. Journal of Molecular Structure, 2013, 1049, 355–361.
14. Salunke-Gawali, S. et al. Synthesis, characterization and molecular structures of homologated analogs of 2-bromo-3-(n-alkylamino)-1,4-napthoquinone. Journal of Molecular Structure, 2014, 1056–1057,

97–103.
15. Frisch, M. et al. Gaussian09 Revision D. 01, Gaussian Inc., Wallingford CT, 2009.R. Dennington, T. Keith, J. Milliam, Semichem. Inc., Shawnee Mission, KS, 2009.
16. Murray J.S., Shields Z.P., Seybold P.G., Politzer P. Intuitive and Counterintuitive Noncovalent Interactions of Aromatic π Regions with the Hydrogen and the Nitrogen of HCN. 2015, J Comp Sci 10:209−216.
17. Lu T, Chen F, Multiwfn: A Multifunctional Wavefunction Analyzer. J Comput Chem, 2012, 33 (5):580−592.
18. Humphrey W, Dalke A, Schulten K., VMD: visual molecular dynamics. J Mol Graphics, 1996, 14, 33−38.
19. Contreras-Garcı´a J, Johnson E.R., Keinan S., Chaudret R., Piquemal J.P., Beratan D.N., Yang W., NCIPLOT: A Program for Plotting Noncovalent Interaction Regions, J Chem Theory Comput , 2011, 7:625–632.
20. Wolff, S. K.; Grimwood, D. J.; McKinnon, J. J.; Turner, M. J.; Jayatilaka, D.; Spackman, M. A. CrystalExplorer 3.1; University of Western Australia: Crawley, Australia, 2012.21.
21. Hirshfeld F.L., Theor. Chim. Acta., 1977, 44 , 129–138.
22. Spackman M.A., Jayatilaka D., Cryst. Eng. Comm., 2009,11, 19–32.
23. Spackman M.A., McKinnon J. J., Cryst. Eng.Comm., 2002,4, 378–392.
24. McKinnon J. J., Spackman M. A., Mitchell A. S., Acta Crystallogr., 2004, B60, 627–668.
25. Rudnick J., Gaspari G., J. Phys. A: Math. Gen. Phys.,1986,19 L191–L193.
26. Baumgartner A., J. Chem. Phys., 1993,99, 7496–7501.